Hydrogen Evolution Reaction Hot Paper

Deutsche Ausgabe: DOI: 10.1002/ange.201604315
Internationale Ausgabe: DOI: 10.1002/anie.201604315

Porous Molybdenum Phosphide Nano-Octahedrons Derived from Confined Phosphorization in UIO-66 for Efficient Hydrogen Evolution

Jian Yang[+], Fengjun Zhang[+], Xin Wang, Dongsheng He, Geng Wu, Qinghua Yang, Xun Hong, Yuen Wu, and Yadong Li**

Abstract: *Herein, a series of porous nano-structured carbocatalysts have been fused and decorated by Mo-based composites, such as Mo_2C, MoN, and MoP, to form a hybrid structures. Using the open porosity derived from the pyrolysis of metal–organic frameworks (MOFs), the highly dispersive MoO_2 small nanoparticles can be deposited in porous carbon by chemical vapor deposition (CVD). Undergoing different treatments of carbonization, nitridation, and phosphorization, the Mo_2C-, MoN-, and MoP-decorated carbocatalysts can be selectively prepared with un-changed morphology. Among these Mo-based composites, the MoP@Porous carbon (MoP@PC) composites exhibited remarkable catalytic activity for the hydrogen evolution reaction (HER) in 0.5 M H_2SO_4 aqueous solution versus MoO_2@PC, Mo_2C@PC, and MoN@PC. This study gives a promising family of multifunctional lab-on-a-particle architectures which shed light on energy conversion and fuel-cell catalysis.*

Recently, the rapid consumption of fossil energy has led to environmental issues, especially global warming and haze. It is urgent to find clean and renewable energy sources to replace fossil energy. Hydrogen (H_2) produced from splitting water by electrochemical process has shown a lot of advantages as a new type of renewable and clean energy.[1] To date, platinum (Pt) has been recognized as one of the most active catalyst for the hydrogen evolution reaction (HER) due to the low Tafel slope and onset potential.[2] However, its high cost and scarce reserves prevents its extensive and practical application.[3] Hence, searching the non-noble-metal HER catalysts can largely remit the environmental and energy issues.[4] Owing to the similar electronic structure as Pt-group metals, transition-metal phosphides, such as tungsten (W) and molybdenum (Mo) phosphides, recently received increasing attention and intensive investigation by more and more researchers.[5] These emerging materials, even the bulk particles or amorphous structure, could exhibit outstanding catalytic performance for HER.[6] Therefore, there is still room to further enhance their properties by decreasing the size of nanoparticles (NPs) and/or regulating the specific nanostructures. The phase-forming temperature of MoP is usually above 800 °C,[6b] thus gaining well-crystallized nanostructured MoP and preventing its aggregation and coalescence at high temperature is still a great challenge.

Metal–organic frameworks (MOFs) are a class of porous materials and have been extensively applied to gas adsorption, separation, sensing, and catalysis.[7] Utilizing their periodic pores and regular architecture, the MOFs could serve as support or counterparts to integrate the active species and finally generate functional hybrid structures.[8] For example, the high surface area and tunable gas adsorption permit the gas harvest on metal surface and acceleration of gas-related catalytic process.[9] The ultrafine porosity can be also used as molecular sieve if the active metal catalysts are fully encapsulated.[10] Beyond that, if the carburization process is limited in carbonaceous matrix, the regular pores of MOFs can effectively host the nanosized Mo-based materials and prevent their agglomeration at high reaction temperatures.

Herein, we demonstrated a MOFs-assisted strategy to develop MoP nanoparticles distributing in porous carbon as efficient HER catalysts. As illustrated in Scheme 1, we select a UIO-66 MOF as the host, whose formula of unit cell is $Zr_{24}O_{120}C_{192}H_{96}$ ($Zr_6O_4(OH)_4(CO_2)_{12}$ as structure building unit (SBU) and 1,4-dicarboxybenzene (H_2BDC) as

[*] J. Yang,[+] X. Wang, D. He, G. Wu, Q. Yang, X. Hong, Y. Wu, Y. Li
Center of Advanced Nanocatalysis, University of Science and Technology of China (CAN-USTC)
Hefei, Anhui 230026 (P.R. China)
and
Department of Chemistry, Tsinghua University
Beijing 100084 (P.R. China)
E-mail: yuenwu@ustc.edu.cn
ydli@mail.tsinghua.edu.cn
J. Yang,[+] F. Zhang[+]
Center of Advanced Nanocatalysis, University of Science and Technology of China (CAN-USTC), Anhui Key Laboratory of Advanced Building Materials, Anhui Jianzhu University
Hefei, Anhui 230026 (P.R. China)
[+] These authors contributed equally to this work.

Supporting information for this article can be found under: http://dx.doi.org/10.1002/anie.201604315.

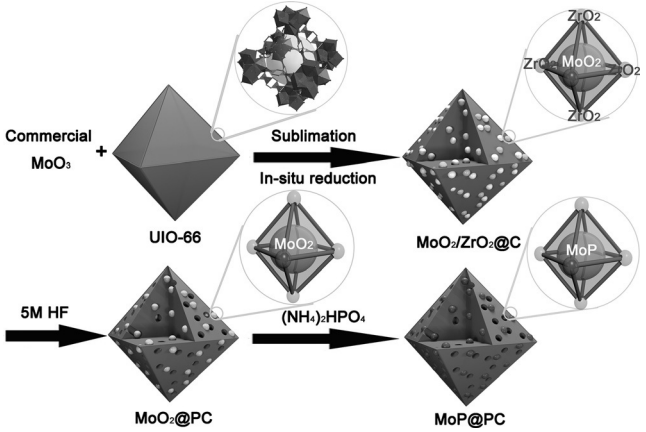

Scheme 1. Preparation process of the MoP@PC nano-octahedrons.

linker).[11] This initial MOF was prepared from the solvothermal reaction, exhibiting uniform octahedral shape and narrow size distribution (Figure S1 in the Supporting Information). Distinct from previous studies, this preparation of Mo-based hybrid used the commercially available MoO_3 (Figure S2) which is easily obtained. Under the CVD condition (Figure S3), the ultrafine pores of UiO-66 (0.6 nm) capture the vaporized MoO_3 which sublimes above 600 °C (Figure S4).[12] Afterwards, the adsorbed MoO_3 species are reduced by the corresponding confined carburization reaction to produce small MoO_2 nanocrystallites. The carburization process effectively avoided the aggregation of MoO_2 nanoparticles (NPs), which is different from the previously reported one-pot strategy.[13] Meanwhile, the SBUs are transferred in situ into the ZrO_2 due to the pyrolysis of carboxylate groups. Furthermore, the inert ZrO_2 NPs were removed by HF solution to expand the surface reactive area. Finally, the MoO_2 NPs are converted into MoP at 850 °C by PH_3 which was generated in situ from the thermal decomposition of $(NH_4)_2HPO_4$.[6b]

As shown in Figure S5, MoO_2 and ZrO_2 nanoparticles within MoO_2/ZrO_2@C both distributed homogeneously in the nano-octahedral carbon and retained their monodispersity. As verified by the missing peaks from X-ray diffraction (XRD) spectra, the inert ZrO_2 nanoparticles were readily etched by HF solution, leaving the monoclinic phase of MoO_2. Thus, a porous nano-octahedral carbon composed of small MoO_2 nanocrystals with a diameter of 3 nm was obtained, which was defined as MoO_2@PC (Figure 1a and Figure S6). The weight percentage of

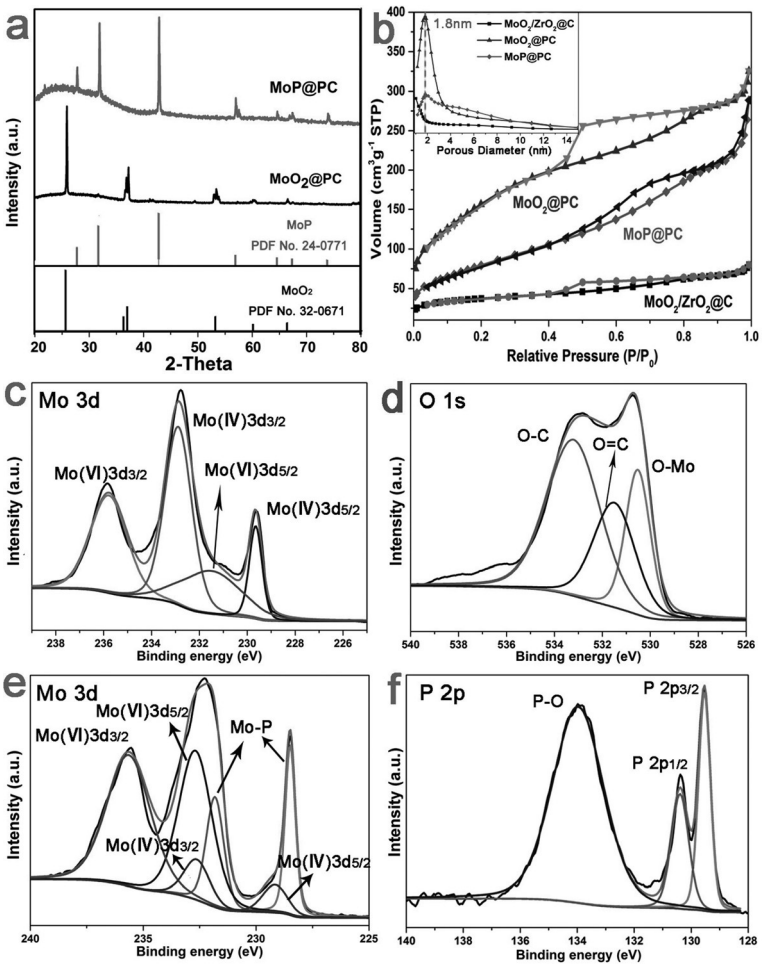

Figure 2. a) XRD pattern of MoO_2@PC and MoP@PC. b) N_2 adsorption/desorption isotherms of MoO_2/ZrO_2@C, MoO_2@PC, and MoP@PC. Inset: the corresponding pore size distribution. XPS spectra of c) Mo 3d, d) O 1s in MoO_2@PC and e) Mo 3d, f) P 2p in MoP@PC.

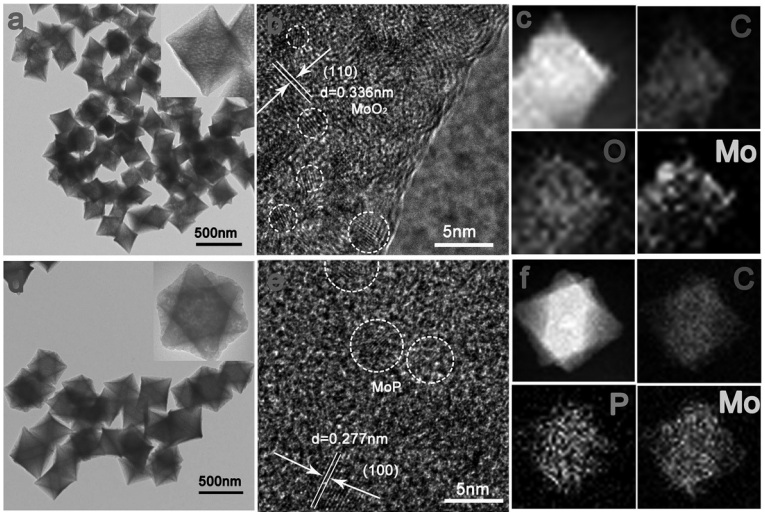

Figure 1. a) TEM image, b) high-resolution TEM image, and c) EDS mapping of MoO_2@PC. d) TEM image, e) high-resolution TEM image, and f) EDS mapping of MoP@PC.

MoO_2 was estimated about 82.8% according to the thermogravimetric (TG) analysis in air (Figure S7). The high resolution TEM image (Figure 1b) clearly showed the MoO_2 nanocrystallites were embedded in the amorphous carbon matrix, whose specific lattice spacing of {110} facet could be measured as 0.336 nm. Careful examinations on different areas confirmed the size of MoO_2 was typically smaller than 4 nm. The elemental mapping was employed to confirm the uniform distribution of Mo, O, and C through the whole octahedrons (Figure 1c). After phosphorization by $(NH_4)_2HPO_4$ heated at 850 °C in H_2/Ar (10%) gas flow, the hybrid of MoO_2@PC was converted in situ into hexagonal MoP@PC, which was verified by XRD pattern in Figure 2a. The reaction that MoO_2 underwent was believed to follow the equation: $2MoO_2 + 2PH_3 + H_2 \rightarrow 2MoP + 4H_2O$. Carful check on TEM images revealed this phosphorization would not result in large MoP NPs that were more than 5 nm within the octahedral support (Figure S8). Moreover, this mild reaction

would not destroy the well-defined octahedral morphology (Figure 1 d and S9), demonstrating the process occurred in the cages of UIO-66. As clearly seen in Figure 1 e, a closer TEM examination locating at the edge of a MoP nano-octahedron gives more details of the lattice fringes of MoP NPs, which was consistent with the d spacing of the (100) planes. The EDS mapping collaboratively support the MoP NPs distributed homogeneously within the whole composites (Figure 1 f).

The BET specific surface area of the as-prepared samples were obtained by recording nitrogen adsorption-desorption isotherms at 77 K (Figure 2 b). The BET surface area of MoO_2/ZrO_2@C, MoO_2@PC, and MoP@PC were 132, 554, and 328 $m^2 g^{-1}$, respectively, demonstrating the treatment by HF could effectively remove the inert ZrO_2 and expand the reactive surface area. It was found nitrogen uptake exhibited a prominent increase at a relative low pressure ($P/P_0 < 0.01$), which indicated the inherent micropores of MoO_2@PC and MoP@PC. This result was consistent with the pore size distribution obtained from adsorption data calculated by BJH method (Figure 2 b, inset), which showed a dominant pore with diameter centering at 1.8 nm for both of MoO_2@PC and MoP@PC. It is worth mentioning there was no clear peak at the curve of pore size distribution for MoO_2/ZrO_2@C. So, the pore centered at 1.8 nm was apparently derived from etching of the ZrO_2 nanoparticles by HF. In addition, the pore distribution and pore volume of (0.341 $cm^3 g^{-1}$) MoP@PC remained unchanged after phosphorization at high temperature.

The X-ray photoelectron spectroscopy (XPS) was further used to characterize the valence state and composition evolution from MoO_2@PC to MoP@PC. The survey spectrum (Figure S10) showed that MoO_2@PC and MoP@PC were composed of Mo, O, C and Mo, P, C, respectively. Figure 2 c indicated four peaks with lower energy spin-spin doublet were attributed to the oxidation state of the Mo^{IV} at 232.9 and 229.7 eV due to Mo ($3d_{3/2}$) and Mo ($3d_{5/2}$), respectively. The peaks at 235.8 and 231.5 eV were assigned to the Mo ($3d_{3/2}$) and Mo ($3d_{5/2}$) of Mo^{VI}, respectively. The O1s peak can be split into three deconvoluted components. Two components at 531.5 and 533.2 eV were O=C and O–C derived from incomplete deoxidization of carboxyl. The third component at 530.5 eV arises from the O–Mo bonds (Figure 2 d).[14] Figure 2 e shows that two doublets at 235.6 eV/232.7 eV (Mo^{VI} $3d_{3/2}/3d_{5/2}$) and 232.6 eV/229.2 eV (Mo^{IV} $3d_{3/2}/3d_{5/2}$) can be assigned to high oxidation state of Mo (MoO_3 and MoO_2).[15] The rest of two double peaks could be ascribed to MoP, which was presented at 231.8 eV and 228.5 eV.[16] Therefore, the surface of small MoP NPs in porous carbon was slightly oxidized, which was due to their high surface energy.[14] This oxidation of MoP was also observed in the XPS spectrum of P 2p. That is, the peak at 134.0 eV could be attributed to PO_4^{3-} or P_2O_5 caused by slightly oxidized P (Figure 2 f).[17] Meanwhile, the doublet (130.4 eV/129.5 eV) can be assigned to P–Mo species in MoP@PC.

With minor modification, this MOFs-assisted strategy to generate Mo-based composites could be readily generalized to other hybrids. For example, Mo_2C and MoN nanoparticles were systematically synthesized under different atmosphere of H_2/Ar (10%) and NH_3 at 800 °C, using MoO_2@PC as precursor. As verified by XRD patterns, the Mo_2C and MoN NPs confined in the mesoporous carbon both exhibited typical hexagonal phase after the transformation. (Figure S11). Furthermore, they both kept the initial porous structure and octahedral morphology. The EDS mapping confirmed the uniform distribution of C, N, Mo and C, Mo, respectively, in the whole nano-octahedral carbon (Figure S12). SEM images revealed the Mo_2C@PC and MoN@PC both exhibited regular octahedral morphology and the average sizes were both 250 nm (Figure S13). Moreover, XPS spectrums further confirm the successful phase evolution from MoO_2 to Mo_2C and MoN, respectively, whose details about valence state can be seen in the Figure S14.

Not only the nanocrystallization of MoP originated from the confinement of porous carbon, but also the extraordinary accessibility and stability endowed by the carbon shell could benefit the application of MoP@PC in electrocatalysis. The electrocatalytic activity of Mo-based composites including MoP@PC, Mo_2C@PC, MoN@PC, and MoO_2@PC were further investigated towards HER. All the loading of electrocatalysts were set to 0.41 mg cm^{-2} on the glassy carbon electrode and the electrocatalysis were all conducted in N_2-saturated 0.5 M H_2SO_4 solution with a scan rate of 50 mV s^{-1}. The representative polarization curves in Figure 3 a indicated the bare porous carbon (PC) and MoO_2@PC both exhibited poor HER activity. The MoP@PC was unexpectedly active for HER. As summarized in Table 1, MoP@PC possessed a lower onset potential of 77 mV compared to Mo_2C@PC (115 mV) and MoN@PC (258 mV). As a comparison, we deliberately synthesized bulk MoP using commercial MoO_3 and $(NH_4)_2HPO_4$ as precursors under the atmosphere of Ar and H_2 (10%) at 850 °C (see details in Supporting Information). Shown in Figure S15, the bulk MoP with hexagonal phase and irregular morphology had been successfully obtained. The current density at 200 mV of MoP@PC was higher than the Mo_2C@PC, MoN@PC, MoO_2@PC, and bulk MoP, revealing its higher electrocatalytic activity. To achieve current density of 10 mA cm^{-2}, the MoP@PC catalyst required smaller overpotential of 153 mV compared to Mo_2C@PC (177 mV), MoN@PC (393 mV) and bulk MoP (217 mV). To further study the HER activity, Figure 3 b clearly showed the Tafel plots which are calculated from polarization curves by Tafel equation. MoP@PC and bulk MoP exhibited the similar Tafel slope, which can be inferred the similar reaction mechanism of MoP@PC and bulk MoP, although the difference in the onset potential and inherent exchange current. In contrast, the Tafel slopes of Mo_2C@PC and MoN@PC were 96 mV dec^{-1} and 167 mV dec^{-1}, respectively, which were quite bigger than that of MoP@PC. Electrochemical impedance spectroscopy (EIS) measurement was adopted to provide further insight into the electrical conductivity of electrocatalysts. MoP@PC showed a small value of charge transfer resistance (26 ohm) due to superior synergistic effect and stronger interaction between the nanosized MoP particles and porous carbon compared to that of Mo_2C@PC (77 ohm) and bulk MoP (124 ohm; Figure 3 c). From Figure S16, the other electrocatalysts showed larger values of charge transfer resistance revealing low HER kinetics at its interface. To

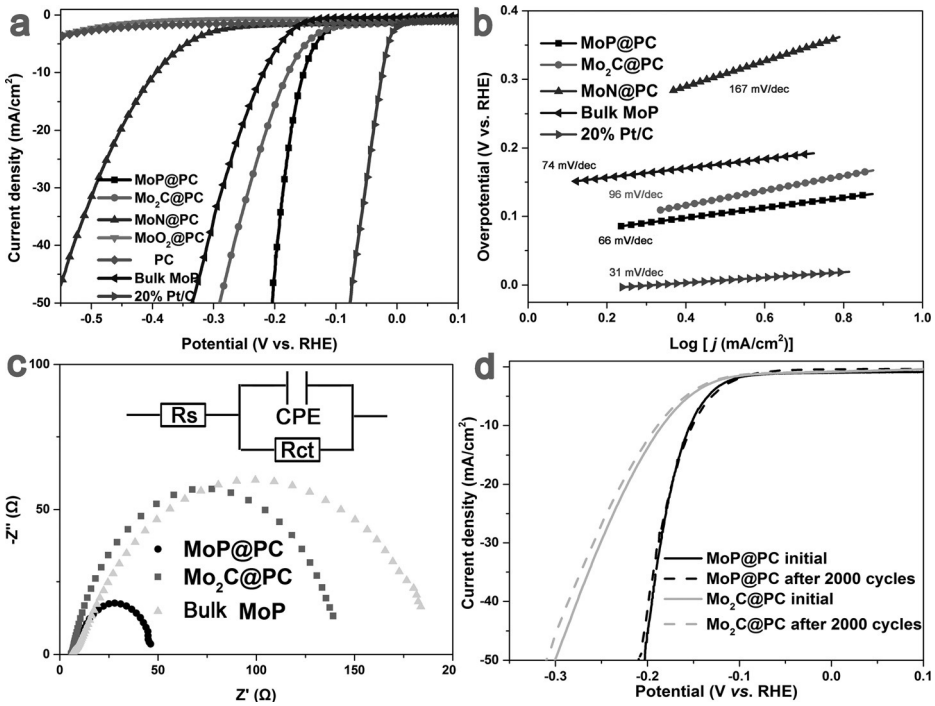

Figure 3. a) Polarization curves for six electrocatalysts. b) Tafel plots calculated from polarization curves. c) EIS (electrochemical impedance spectra) of three electrocatalysts. Rs and Rct represent the electrolyte, charge transfer resistance, respectively. d) Durability of MoP@PC and Mo_2C@PC.

Table 1: Summary of electrocatalytic performance of four catalysts.

Catalyst	Onset Potential [mV][a]	Tafel slope [mV*dec^{-1}]	η_{10} [mA cm^{-2}][a]	J_0 [A cm^{-2}][b]
MoP@PC	77	66	153	2.1×10^{-4}
Mo_2C@PC	115	96	177	1.6×10^{-4}
MoN@PC	258	167	393	8.5×10^{-5}
Bulk MoP	125	74	217	1.3×10^{-5}

[a] The potential measured versus RHE. [b] J_0 values were calculated from Tafel curves using an extrapolation method.

assess the durability of MoP@PC and Mo_2C@PC, accelerated linear potential sweeps were conducted repeatedly on the electrodes (Figure 3d). Mo_2C@PC both exhibited a continuous but small loss of activity on repeated potential sweeps, implying minor corrosion of electrocatalysts in the acid condition. Meanwhile, the rapid rotation could also be responsible for the degradation of the catalytic performance.[4b] In contrast, there was no obvious activity decay observed for the durability test of MoP@PC. Furthermore, these Mo-based compositions were investigated in 1M KOH solution (Figure S17). As shown, the MoP@PC, Mo_2C@PC and MoN@PC all showed comparable HER activity, although the poor activity of MoO_2@PC can be found.

In summary, a series of Mo-based nanostructures, such as MoO_2, Mo_2C, MoN and MoP, have been successfully synthesized by a MOFs-assisted strategy as highly active electrocatalysts for HER. This strategy relies on the in situ carburization, nitridation, and phosphorization reactions on commercial MoO_3 which were confined in the ultrafine pores of UIO-66. The MoP@PC shows remarkable electrocatalytic activity and stability for HER versus Mo_2C@PC, MoN@PC, MoO_2@PC, and bulk MoP, benefiting from the outstanding size effect of small nanoparticles and highly exposed and accessible surface area. Our findings opened a new opportunities to synthesize other MOFs-based composites for various applications.

Acknowledgements

This work was supported by the Fundamental Research Funds for the Central Universities (WK2060190043), National Natural Science Foundation of China (21521091, 21131004, 21390393, U1463202 and 21522107).

Keywords: hydrogen evolution reaction · metal–organic frameworks · molybdenum · nanoparticles · porous carbons

How to cite: *Angew. Chem. Int. Ed.* **2016**, *55*, 12854–12858
Angew. Chem. **2016**, *128*, 13046–13050

[1] J. A. Turner, *Science* **2004**, *305*, 972–974.
[2] J. R. McKone, E. L. Warren, M. J. Bierman, S. W. Boettcher, B. S. Brunschwig, N. S. Lewis, H. B. Gray, *Energy Environ. Sci.* **2011**, *4*, 3573–3583.
[3] H. B. Gray, *Nat. Chem.* **2009**, *1*, 112–112.
[4] a) M. R. Gao, J. X. Liang, Y. R. Zheng, Y. F. Xu, J. Jiang, Q. Gao, J. Li, S. H. Yu, *Nat. Commun.* **2015**, *6*, 5982–5988; b) H. B. Wu, B. Y. Xia, L. Yu, X. Y. Yu, X. W. Lou, *Nat. Commun.* **2015**, *6*, 6512–6519; c) H. J. Yan, C. G. Tian, L. Wang, A. P. Wu, M. C. Meng, L. Zhao, H. G. Fu, *Angew. Chem. Int. Ed.* **2015**, *54*, 6325–6329; *Angew. Chem.* **2015**, *127*, 6423–6427; d) F. X. Ma, H. B. Wu, B. Y. Xia, C. Y. Xu, X. W. Lou, *Angew. Chem. Int. Ed.* **2015**, *54*, 15395–15399; *Angew. Chem.* **2015**, *127*, 15615–15619; e) H. T. Wang, C. Tsai, D. S. Kong, K. R. Chan, F. Abild-Pedersen, J. Norskov, Y. Cui, *Nano Res.* **2015**, *8*, 566–575; f) J. Kibsgaard, C. Tsai, K. Chan, J. D. Benck, J. K. Norskov, F. Abild-Pedersen, T. F. Jaramillo, *Energy Environ. Sci.* **2015**, *8*, 3022–3029; g) H. Li, C. Tsai, A. L. Koh, L. L. Cai, A. W. Contryman, A. H. Fragapane, J. H. Zhao, H. S. Han, H. C. Manoharan, F. Abild-Pedersen, J. K. Norskov, X. L. Zheng, *Nat. Mater.* **2016**, *15*, 48–53; h) S. C. Lee, J. D. Benck, C. Tsai, J. Park, A. L. Koh, F. Abild-Pedersen, T. F. Jaramillo, R. Sinclair, *ACS Nano* **2016**, *10*, 624–632.
[5] a) P. Jiang, Q. Liu, Y. H. Liang, J. Q. Tian, A. M. Asiri, X. P. Sun, *Angew. Chem. Int. Ed.* **2014**, *53*, 12855–12859; *Angew. Chem.* **2014**, *126*, 13069–13073; b) J. M. McEnaney, J. C. Crompton, J. F. Callejas, E. J. Popczun, A. J. Biacchi, N. S. Lewis, R. E. Schaak, *Chem. Mater.* **2014**, *26*, 4826–4831; c) J. M. McEnaney, J. C. Crompton, J. F. Callejas, E. J. Popczun, C. G. Read, N. S. Lewis, R. E. Schaak, *Chem. Commun.* **2014**, *50*, 11026–11028; d) Z. H. Pu, Q. Liu, A. M. Asiri, X. P. Sun, *ACS Appl. Mater.*

Interfaces **2014**, *6*, 21874 – 21879; e) P. Wang, F. Song, R. Amal, Y. H. Ng, X. Hu, *ChemSusChem* **2016**, *9*, 472 – 477.

[6] a) J. Kibsgaard, T. F. Jaramillo, *Angew. Chem. Int. Ed.* **2014**, *53*, 14433 – 14437; *Angew. Chem.* **2014**, *126*, 14661 – 14665; b) Z. C. Xing, Q. Liu, A. M. Asiri, X. P. Sun, *Adv. Mater.* **2014**, *26*, 5702 – 5707.

[7] a) H. Furukawa, K. E. Cordova, M. O'Keeffe, O. M. Yaghi, *Science* **2013**, *341*, 1230444 – 1230455; b) R. J. Kuppler, D. J. Timmons, Q. R. Fang, J. R. Li, T. A. Makal, M. D. Young, D. Q. Yuan, D. Zhao, W. J. Zhuang, H. C. Zhou, *Coord. Chem. Rev.* **2009**, *253*, 3042 – 3066.

[8] a) H. Hu, L. Han, M. Z. Yu, Z. Y. Wang, X. W. Lou, *Energy Environ. Sci.* **2016**, *9*, 107 – 111; b) B. Y. Xia, Y. Yan, N. Li, H. B. Wu, X. W. Lou, X. Wang, *Nat. Energy* **2016**, *1*, 15006 – 15013.

[9] a) G. Q. Li, H. Kobayashi, J. M. Taylor, R. Ikeda, Y. Kubota, K. Kato, M. Takata, T. Yamamoto, S. Toh, S. Matsumura, H. Kitagawa, *Nat. Mater.* **2014**, *13*, 802 – 806; b) J. Yang, F. J. Zhang, H. Y. Lu, X. Hong, H. L. Jiang, Y. E. Wu, Y. D. Li, *Angew. Chem. Int. Ed.* **2015**, *54*, 10889 – 10893; *Angew. Chem.* **2015**, *127*, 11039 – 11043.

[10] a) C. H. Kuo, Y. Tang, L. Y. Chou, B. T. Sneed, C. N. Brodsky, Z. P. Zhao, C. K. Tsung, *J. Am. Chem. Soc.* **2012**, *134*, 14345 – 14348; b) Z. Li, R. Yu, J. L. Huang, Y. S. Shi, D. Y. Zhang, X. Y. Zhong, D. S. Wang, Y. E. Wu, Y. D. Li, *Nat. Commun.* **2015**, *6*, 8248 – 8255; c) W. N. Zhang, G. Lu, C. L. Cui, Y. Y. Liu, S. Z. Li, W. J. Yan, C. Xing, Y. R. Chi, Y. H. Yang, F. W. Huo, *Adv. Mater.* **2014**, *26*, 4056 – 4060.

[11] J. H. Cavka, S. Jakobsen, U. Olsbye, N. Guillou, C. Lamberti, S. Bordiga, K. P. Lillerud, *J. Am. Chem. Soc.* **2008**, *130*, 13850 – 13851.

[12] A. Malinowski, R. Ohnishi, M. Ichikawa, *Catal. Lett.* **2004**, *96*, 141 – 146.

[13] Y. J. Tang, M. R. Gao, C. H. Liu, S. L. Li, H. L. Jiang, Y. Q. Lan, M. Han, S. H. Yu, *Angew. Chem. Int. Ed.* **2015**, *54*, 12928 – 12932; *Angew. Chem.* **2015**, *127*, 13120 – 13124.

[14] A. Bhaskar, M. Deepa, T. N. Rao, *ACS Appl. Mater. Interfaces* **2013**, *5*, 2555 – 2566.

[15] P. Xiao, M. A. Sk, L. Thia, X. M. Ge, R. J. Lim, J. Y. Wang, K. H. Lim, X. Wang, *Energy Environ. Sci.* **2014**, *7*, 2624 – 2629.

[16] a) D. C. Phillips, S. J. Sawhill, R. Self, M. E. Bussell, *J. Catal.* **2002**, *207*, 266 – 273; b) X. Y. Zhao, M. H. Cao, B. Liu, Y. Tian, C. W. Hu, *J. Mater. Chem.* **2012**, *22*, 13334 – 13340.

[17] J. Bai, X. Li, A. J. Wang, R. Prins, Y. Wang, *J. Catal.* **2012**, *287*, 161 – 169.

Received: May 3, 2016
Published online: July 7, 2016

